NANO LETTERS

2005
Vol. 5, No. 10
1972−1977

The Structures of Ag_{55}^{+} and Ag_{55}^{-}: Trapped Ion Electron Diffraction and Density Functional Theory

Detlef Schooss,*,† Martine N. Blom,† Joel H. Parks,‡ Bernd v. Issendorff,§ Hellmut Haberland,§ and Manfred M. Kappes†,||

Institut für Nanotechnologie, Forschungszentrum Karlsruhe, Postfach 3640, 76021 Karlsruhe, Germany, Rowland Institute at Harvard, 100 Edwin H. Land Boulevard, Cambridge, Massachusetts 02142, Fakultät für Physik, Universität Freiburg, Herman Herderstrasse 3, D-79104 Freiburg, Germany, and Institut für Physikalische Chemie, Universität Karlsruhe, Kaiserstr.12, 76128 Karlsruhe, Germany

Received July 14, 2005; Revised Manuscript Received August 30, 2005

ABSTRACT

We report the experimental structure determination of cold, mass selected $Ag_{55}^{+/-}$ cluster ions using the recently developed technique of trapped ion electron diffraction. By comparison of experimental and theoretical molecular scattering functions and consideration of computed total energies, we show that Ag_{55}^{+} constitutes an ideal Mackay icosahedron, whereas Ag_{55}^{-} is a weakly Jahn–Teller distorted icosahedron. Isomers of other structural types, for example, decahedral or close-packed, could be ruled out. The candidate structures were obtained by density functional theory calculations.

Metal clusters are intermediate in size between atoms and microscopic pieces of the bulk metal. They often show strongly size dependent physical[1−4] and chemical[5] properties. These size-dependent properties are not only of fundamental interest but also of practical relevance to heterogeneous catalysis and nanotechnology. Many characteristics of a metal cluster are determined by its geometric structure, making structure determination an important step in understanding cluster properties; in particular, equilibrium structures commonly deviate significantly from simple segments of the bulk lattice. Even before the discovery of fullerenes, predictions and indirect experimental inferences of high-symmetry closed-shell structures for specific metal cluster sizes have fueled efforts to develop size-specific experimental structure determination methods for free mass-selected clusters. Photodissociation spectra in combination with the calculation of absorption spectra have been used to assign structures for small clusters.[6−11] Structures of metal clusters $M_n^{+/-}$ with $n < 20$ have also been determined by ion mobility measurements in combination with ab initio calculations.[12,13] The ion mobility method is sensitive to the collision cross section of a cluster and is therefore most effectively used for smaller metal clusters. Photoelectron spectroscopy (PES) has also been applied to the structure assignment of small- and medium-sized metal cluster anions.[14−16] PES is sensitive to the electron density of states and in conjunction with ab initio calculations gives unambiguous structural information particularly in high-symmetry cases.

A complementary and more direct method of structure determination is the recently developed technique of trapped ion electron diffraction (TIED) that we apply in this study.[17,18] Because of the diffraction nature of TIED, the method is especially sensitive to the number of nearest neighbors as well as to the next neighbor distances. TIED allows structural assignment via comparison to trial structures derived from theory. Here we have chosen to apply TIED to mid-size silver clusters because these currently provide optimum theoretical/experimental tractability and nanotechnological interest. Note that electron diffraction studies have been performed previously on wide size and internal energy distributions of neutral silver clusters in a supersonic beam.[19−23] Although this work suggested the presence of icosahedral-type clusters (in contrast to segments of bulk silver (fcc)) in the ensemble, the method did not allow structure determination for specific sizes. Below we study a single silver cluster size at a well-defined temperature in two different charge states, $Ag_{55}^{+/-}$. By comparison of TIED data to trial structures deriving from DFT calculations, we demonstrate that both Ag_{55}^{+} and Ag_{55}^{-}, as probed in our experiment, have closed-shell icosahedral molecular structures.

* Corresponding author: E-mail: detlef.schooss@int.fzk.de.
† Institut für Nanotechnologie.
‡ Rowland Institute at Harvard.
§ Fakultät für Physik, Universität Freiburg.
|| Institut für Physikalische Chemie, Universität Karlsruhe.

10.1021/nl0513434 CCC: $30.25
Published on Web 09/23/2005

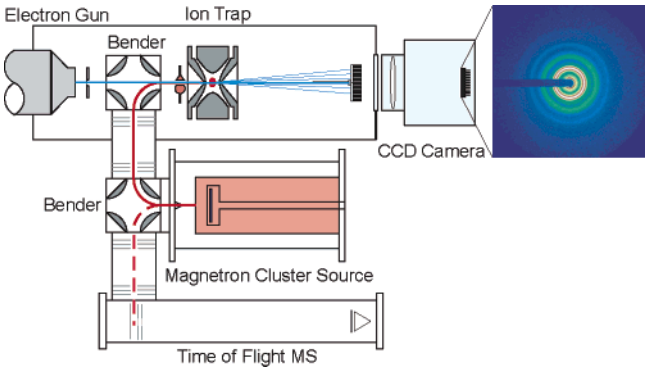

Figure 1. Experimental arrangement for trapped ion electron diffraction. Cluster ions are generated in a magnetron sputter cluster source and trapped in the quadrupole ion trap. Electrons from the electron gun are diffracted by the cluster ions and the scattering pattern is detected using a phosphor screen CCD camera combination. The CCD is mounted outside the UHV chamber. Also shown is a raw CCD image (in false colors) of Ag_{55}^+ diffraction data after subtraction of the reference image (right).

The components of the trapped ion electron diffraction (TIED) apparatus are shown schematically in Figure 1. It comprises a home-built quadrupole ion trap with an inner diameter of the ring electrode of 14.1 mm and an end-cap spacing of 10.8 mm. A radio frequency (300 kHz) voltage of up to 5000 V_{0P} is applied to the ring, while the end caps remain grounded. The trap electrodes are attached to a heater/cooler assembly allowing temperature control of the trap between 90 and 450 K. A long focal length electron gun (VTS-Createc) generates a well-collimated electron beam of 0.5-mm diameter at a kinetic energy of 40 keV (λ = 0.0601 Å). The electron beam passes through the trap via 1.5-mm-diameter holes in the end caps, allowing for a maximum scattering angle $\vartheta_{max} = 7.7°$, which corresponds to a maximum scattering vector of $s_{max} = 14.5$ Å^{-1}. While the primary beam is captured in a Faraday cup, diffracted electrons are detected on a phosphorescent screen assembly, which is imaged on a liquid-nitrogen-cooled CCD camera (Roper Scientific) external to the UHV chamber.

Silver cluster ions were produced by an inert gas condensation cluster source based on a DC magnetron sputtering process developed by Haberland and co-workers.[24] The cluster source operated at 90 K using a gas mixture of ~10 vol % Ar (99.999%) in He (99.9999%) at a total pressure of ca. 1 mbar. A silver target of 99.99% purity was used. The intensity and purity of the cluster ions were optimized and monitored by a linear time-of-flight mass spectrometer.

The cluster ions generated were injected into the trap via two quadrupole benders and associated ion optics collinear to the electron beam. Mass selection to a single cluster size (i.e., no detectable neighbor cluster sizes) prior and during the diffraction period was achieved by applying a dipolar SWIFT excitation[25,26] via the endcaps of the trap. On the order of 10^5 cluster ions were captured from the ion beam, mass selected, and thermalized for 1−2 s in a He bath at approximately 10^{-3} mbar. After pump down to 10^{-9} mbar, the ion cloud was irradiated by the electron beam for an exposure time of typically 30 s at an electron beam current of ca. 1 μA. During the diffraction period, all of the fragmentation products (e.g., caused by inelastic scattering and subsequent heating and dissociation of the trapped clusters) were removed by continuous SWIFT excitation to ensure strict size selectivity. To account for the experimental background, we accumulated a reference exposure by repeating exactly the same sequence without cluster ions in the trap (alternating cluster signal and reference exposures). The number of signal exposures for a cluster size was approximately 400, corresponding to a total measurement time of 6−8 h. All of the measurements shown here were performed at a trap temperature of (95 ± 1) K.

Reference and cluster signal exposures were averaged separately, and the averages were subtracted from each other. This yielded a difference picture that was subsequently centered and radially averaged to obtain the total diffraction intensity I_{tot}^{exp} as a function of the electron momentum transfer $s = 4\pi/\lambda \sin(\theta/2)$ where θ is the scattering angle and λ is the electron wavelength. The experimental reduced molecular scattering intensity sM^{exp} can be defined by[27]

$$sM^{exp}(s) = s\left(\frac{I_{tot}^{exp}}{I_{at}\, I_{back}} - 1\right) \tag{1}$$

with the atomic scattering contribution I_{at} and an additional unspecific background I_{back}, defined as a "flat" function of the form[28]

$$I_{back}(s) = A\exp(-\alpha s) + \sum_{i=0}^{4} a_i\, s^i \tag{2}$$

This background is caused by extraneous scattering (e.g., inelastic scattering) and is not separately determinable. The parameters of the background function (A, α, a_i) are varied independently and optimized in the fitting procedure described below.

In the case of a homoatomic cluster, the theoretical reduced molecular scattering function sM^{theo} can be written as

$$sM^{theo}(s') = \frac{S_c}{N}\exp\left(-\frac{L^2}{2}s'^2\right)\sum_i \sum_{j\neq i}\frac{\sin(r_{ij}\, s')}{r_{ij}} \tag{3}$$

where N is the number of atoms in the cluster and r_{ij} is the distance between atom pair i and j. The mean squared vibrational amplitude, L, is included to express the attenuation of the interference term contributed mainly by thermal vibrations. In this simple model it is assumed that the displacement of atoms is random and isotropic about their equilibrium positions. In this case, L is the rms displacement averaged over all atom pairs in the cluster. In addition to the amplitude scaling factor, S_c, a scaling factor for the s scale, k_s, is used where $s' = k_s s$.

The experimental data is broadened by the finite electron beam width in the scattering region, by the finite distribution of scatterers, and by the angular variation of the electron

beam. To include these broadening effects in modeling the experimental data, we smoothed the theoretical molecular diffraction intensity before analysis by a moving average over $\Delta s = 0.39$ Å^{-1}. The differences between the model and experimental scattering intensities were then minimized by a χ^2 fit of S_c, k_s, and L as well as the parameters of the background function. The quality of the fit, that is, the level of agreement between sM^{exp} and sM^{theo}, is characterized by a weighted R-value of the form

$$R_w = \sqrt{\frac{\sum_i w_i \left(sM_i^{\mathrm{theo}} - sM_i^{\mathrm{exp}}\right)^2}{\sum_i w_i \left(sM_i^{\mathrm{exp}}\right)^2}} \qquad (4)$$

The sums go over all of the experimental and corresponding theory data points. The weighting factors, $w_i = 1/\sigma^2_{sM,i}$, are calculated from the (error propagated) standard deviation of $I_{\mathrm{tot}}^{\mathrm{exp}}$.

All of the calculations were performed with the TURBOMOLE[29] package using the DFT level of theory with the S-VWN+Becke-Perdew parametrization (BP-86) and the resolution of the identity approximation for the Coulomb energy (RI-J) quadrature.[30−32] We use a split valence plus polarization (SVP) basis set ((7s6p5d)/[5s3p2d]) along with a scalar relativistic effective core-potential (RECP) that retains 19 electrons in the valence space.[33] For the clusters studied, pure spin states with deviations $\langle S^2 \rangle$ of less than about 0.1 from the exact values were always obtained.

Although a systematic search for the global minimum structure in this size range has been shown to be promising for semiempirical potential functions,[34,35] this is currently prohibitively expensive for DFT calculations. Instead, only a limited number of structures were considered as starting points for geometry optimization. These structures were chosen to reflect different possible structural motifs (e.g., icosahedral, decahedral or close packed), partially with the aid of the WWW based Cambridge Cluster Database.[36] Corresponding DFT calculations allowed for structure relaxation (energy minimization) under the symmetry constraint of the starting geometry.

Small silver clusters have been extensively studied theoretically.[13,37−40] The medium size range including $Ag_{55}^{+/-}$ has been modeled using semiempirical interatomic (Gupta[41] or Sutton Chen[42]) potentials. These favor icosahedral structures. Neutral[43] and anionic[16] Ag_{55} clusters have also been treated with density functional calculations, with the closed-shell icosahedron being the lowest energy isomer found for both charge states. The density of states calculated in the anion DFT study fits well with the experimental photoelectron spectrum obtained in the same work.[16]

Arranging 55 atoms in a closed shell leads to (at least) three possible topologies: a Mackay icosahedron (ico), a truncated decahedron (trdec), and a cuboctahedron (cubo), see Figure 2. Of these, the lowest energy isomer for Ag_{55}^{+} is the icosahedron (see Table 1). At the DFT level, the tentative ground state of Ag_{55}^{+} is a high spin state with the full I_h symmetry (the HOMO is an energetically well separated half filled g_g^4 orbital). However, the Jahn−Teller distorted singlet state with reduced symmetry D_{5d} is isoenergetic. A further reduction of symmetry does not lead to a decrease in energy. The other closed-shell structures, the truncated decahedron (trdec-D_{5h}) and the cuboctahedron (cubo-C_{4v}), are 0.9 and 2.1 eV, respectively, above the proposed ground state.

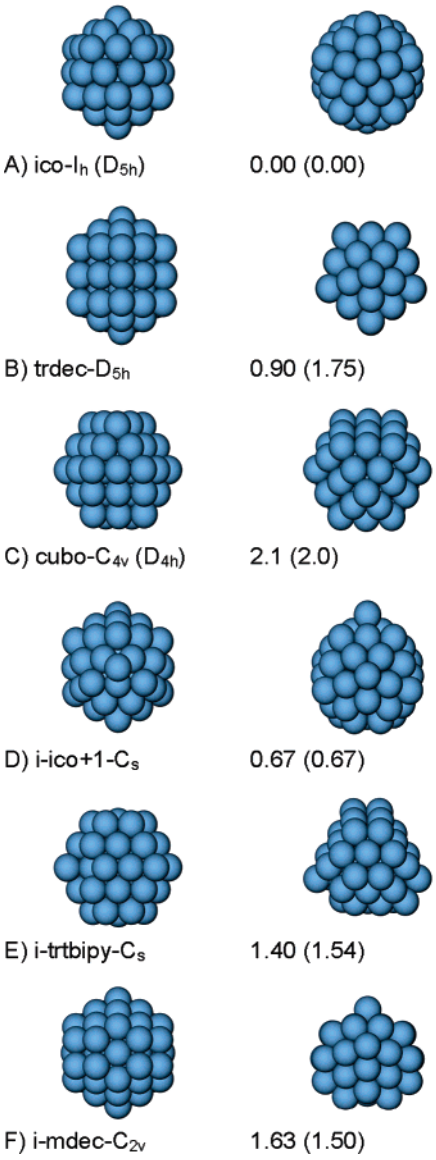

Figure 2. Minimum energy forms found for various $Ag_{55}^{+/-}$ structure types using DFT calculations (see text). Shown are the optimized structures (side-view left, top-view right) together with point group symmetries and relative stabilities for Ag_{55}^{+} (Ag_{55}^{-}) in eV. (A) icosahedral, (B) truncated decahedral, (C) cuboctahedral, (D) incomplete Mackay icosahedron with surface adatom, (E) incomplete trigonal bipyramid, and (F) incomplete Marks decahedron.

For comparison, a single defect Mackay icosahedron was generated by removing an atom from a vertex of the closed-shell icosahedron and placing it on the center of a face. Of the possible adatom-site isomers unrelated by symmetry, the

Table 1. Calculated Properties and Experimental R_w values of Ag_{55}^+ Isomers[a]

type	G	HOMO	state	ΔE/eV	R_w
ico	I_h	g_g^4	^5A_g	0.00	5.1
ico	D_{5d}	e_{1g}^4	$^1A_{1g}$	0.00	5.0
i-ico + 1	C_s	a'^2	$^1A'$	0.67	5.2
trdec	D_{5h}	$e_1''^4$	$^1A_1'$	0.90	21
i-trtbipy	C_s	a'^2	$^1A'$	1.40	26
i-mdec	C_{2v}	a_1^2	$^1A_1$	1.63	17
cubo	C_{4v}	e^4	$^1A_1$	2.10	37

[a] The cluster type is defined in the text. G denotes the symmetry point group, HOMO is the highest occupied molecular orbital. Also listed are the spin state and ΔE, the relative stability with respect to the most stable isomer. The R_w value is defined in the text and given in percent.

Table 2. Calculated Properties and Experimental R_w values of Ag_{55}^- Isomers[a]

type	G	HOMO	state	ΔE/eV	R_w
ico	D_{3d}	e_g^4	$^1A_{1g}$	0.00	6.5
ico	D_{5h}	e_{2g}^2	$^3A_{2g}$	0.04	7.0
i-ico + 1	C_s	a'^2	$^1A'$	0.67	5.9
trdec	D_{5h}	$e_1'^2$	$^3A_2'$	1.75	18
i-trtbipy	C_s	a'^2	$^1A'$	1.54	23
i-mdec	C_{2v}	b_1^2	$^1A_1$	1.50	17
cubo	D_{4h}	t_{1g}^6	$^1A_{1g}$	2.01	35

[a] Abbreviations as in Table 1.

one with lowest energy is 0.67 eV above the I_h ground state and shown in Figure 2 (i-ico+1-C_s). Other open geometry structures were also calculated. Of these, two of the lower lying isomers are the incomplete truncated trigonal bipyramid (i-trtbipy-C_s) composed of fcc layers with a stacking error and the i-mdec-C_{2v} isomer, which is a part of the 75-atom Marks decahedron,[44] 1.4 and 1.6 eV above the I_h isomer, respectively.

For Ag_{55}^-, the energy ordering of the closed-shell structures is very similar (see Table 2). The slightly Jahn−Teller distorted singlet iscosahedral isomer with D_{3d} symmetry is the tentative ground state. The triplet state with D_{5h} symmetry is almost isoenergetic. The decahedral and cuboctahedral isomers, as well as open shell structures are again clearly higher in energy than the icosahedral isomers.

As a typical example, Figure 3 shows the total scattering intensity for Ag_{55}^+ after subtraction of reference exposures, center finding, and ring averaging. The error bars in Figure 3 indicate the standard deviation ($\pm\sigma$) of the circular averaging. No additional averaging or smoothing was applied to the experimental data. For each trial structure considered, S_c, k_s, and L as well as the parameter of the background function was fitted to the experimental data. The resultant best fits are shown in Figure 4A−C for three different closed-shell trial structures of Ag_{55}^+. Note that, in general, sM^{exp} is slightly dependent on the trial structure. This is caused by the simultaneous fitting of background and sM^{theo} to sM^{exp}. However, because the background is a flat function of a frequency much lower than the lowest frequency of the data, this dependence is weak and does not hinder the structural assignment.

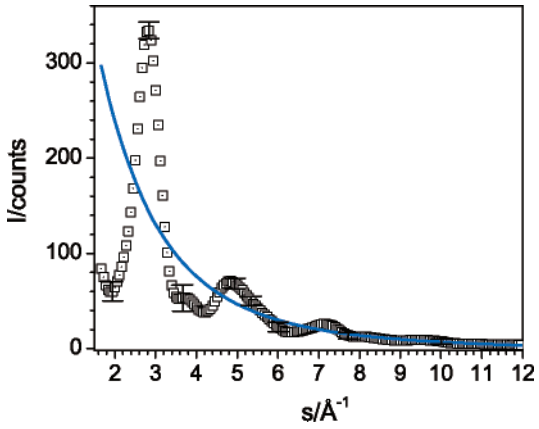

Figure 3. Total experimental scattering intensity, I_{tot}^{exp} (open squares), and the product of atomic and background scattering, $I_{at}I_{back}$ (line), as a function of the momentum transfer s for Ag_{55}^+. The error bars show the standard deviation ($\pm\sigma$).

Comparing the R_w values of the different model structures (Tables 1 and 2) reveals that the cluster distribution probed (ca. 10^5 ions per exposure) can be well described in terms of only one structural motif. For Ag_{55}^+ and Ag_{55}^- (see Figure 4), this structural motif is clearly that of the icosahedron. The agreement of experimental and simulated molecular scattering function is excellent for the iscosahedral structures (R_w = 5.5% and 6.5%), all other structural motifs can be ruled out as significant contributors based on the much higher R_w values. This is, in turn, in very good agreement with the RIDFT calculation suggesting that only the lowest energy forms of $Ag_{55}^{+/-}$ are generated and probed in experiment under our conditions.

Note that the differences in the structures and the reduced molecular scattering functions of the icosahedral isomers of $Ag_{55}^{+/-}$ are minimal and within the experimental error, as are the differences between the Ag_{55} charge states (see Figure 4 A,D and Table 3).

In comparing experimental and theoretical intensities, the only structural variation that was allowed from calculated atomic coordinates is a uniform volume compression (or dilatation) via the s-scaling factor k_s. The best fits for the icosahedral structures were obtained with an inward displacement from the optimized structures by 4.7% (Table 3). The maximum systematic error of k_s, which is determined mainly by the uncertainty of the dimensions of the scattering geometry, is less than 3%. The remaining discrepancies between measured and calculated data could be attributed here to a DFT deficiency in accordance with the observed trend of overestimating bond distances in such calculations.[45]

The structures of free mass-selected Ag_{55}^+ and Ag_{55}^- were investigated by trapped ion electron diffraction at 95 K. The experimental data were best described by a closed-shell icosahedron, as modeled with DFT calculations. Other structural motifs were ruled out on the basis of disagreement of experimental and simulated molecular diffraction functions. Our data are in good agreement with a recent PES study of Ag_{55}^-, which made use of an identical cluster source.[16] Low-temperature trapped ion electron diffraction appears well-suited to molecular structure determination for

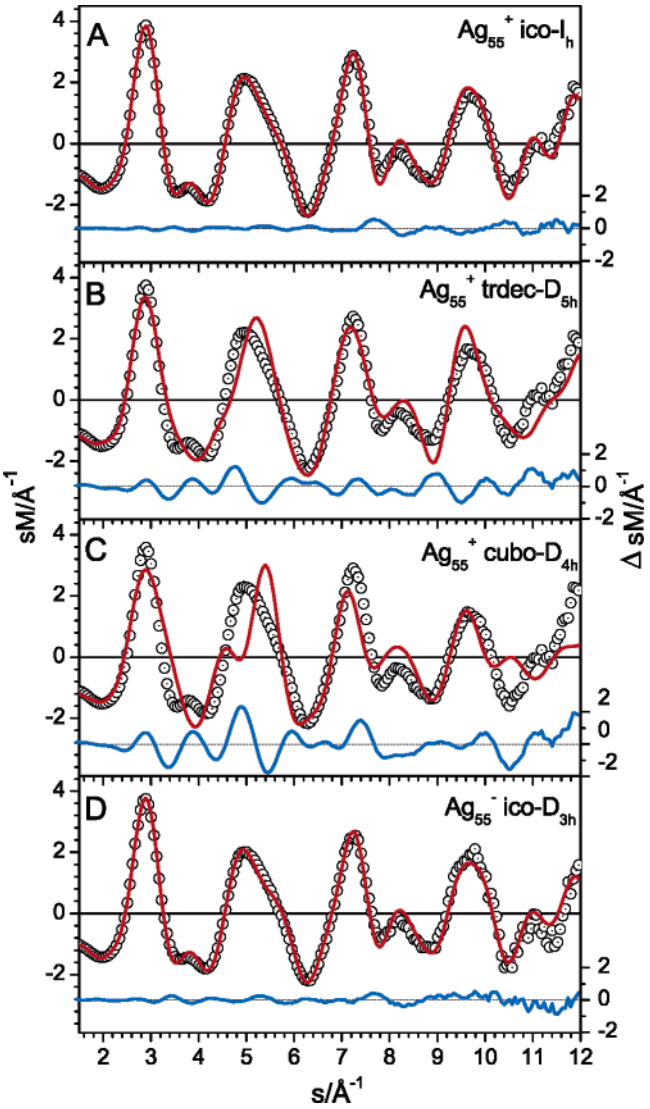

Figure 4. Comparison of the experimental (open circles) and model (line) reduced molecular scattering functions for the icosahedral ico-I_h (A), the truncated decahedral (B), and the cuboctahedral (C) isomers of Ag_{55}^{+} and for the icosahedral isomer of Ag_{55}^{-} (D). The lower traces show the residuals. All of the measurements were performed at a trap temperature of (95 ± 1) K.

Table 3. Ag_{55}^{+}/Ag_{55}^{-} Icosahedral Model Fitting Parameter

	symmetry	S_c	L	k_s
Ag_{55}^{+}	I_h	0.897	0.106	1.0471
Ag_{55}^{-}	D_{3d}	0.894	0.111	1.0468

isolated transition metal cluster ions. TIED is also able to gauge the accuracy of present quantum chemical methods as applied to such systems.[47]

Acknowledgment. This research was supported by the Forschungszentrum Karlsruhe and by the Deutsche Forschungsgemeinschaft as administered through the Center for Functional Nanostructures (CFN). D.S. and M.N.B. thank R. Ahlrichs for helpful discussions regarding the RIDFT calculations, L. Walter for his help in setting up the experiment, and W. Hill for his help with the trap electronics.

References

(1) de Heer, W. A. *Rev. Mod. Phys.* **1993**, *65*, 611−676.
(2) Schmidt, M.; Kusche, R.; Issendorff, B. v.; Haberland, H. *Nature* **1989**, *393*, 238.
(3) Martin, T. P. *Phys. Rep.* **1996**, *273*, 199−241.
(4) Baletto, F.; Ferrando, R. *Rev. Mod. Phys.* **2005**, *77*, 371.
(5) Heiz, U.; Schneider, W. D. *J. Phys. D: Appl. Phys.* **2000**, *33*, R85−R102.
(6) Jarrold, M. F.; Creegan, K. M. *Chem. Phys. Lett.* **1990**, *166*, 116−122.
(7) Wang, C. R. C.; Pollack, S.; Dahlseid, T. A.; Koretsky, G. M.; Kappes, M. M. *J. Chem. Phys.* **1992**, *96*, 7931−7937.
(8) Ikegami, T.; Kondow, T.; Iwata, S. *J. Chem. Phys.* **1993**, *98*, 3038−3048.
(9) Pellarin, M.; Cottancin, E.; Lerme, J.; Vialle, J. L.; Broyer, M.; Tournus, F.; Masenelli, B.; Melinon, P. *J. Chem. Phys.* **2002**, *117*, 3088−3097.
(10) Schooss, D.; Gilb, S.; Kaller, J.; Kappes, M. M.; Furche, F.; Kohn, A.; May, K.; Ahlrichs, R. *J. Chem. Phys.* **2000**, *113*, 5361−5371.
(11) Fielicke, A.; Mitric, R.; Meijer, G.; Bonacic-Koutecky, V.; von Helden, G. *J. Am. Chem. Soc.* **2003**, *125*, 15716−15717.
(12) Gilb, S.; Weis, P.; Furche, F.; Ahlrichs, R.; Kappes, M. M. *J. Chem. Phys.* **2002**, *116*, 4094−4101.
(13) Weis, P.; Bierweiler, T.; Gilb, S.; Kappes, M. M. *Chem. Phys. Lett.* **2002**, *355*, 355−364.
(14) Kietzmann, H.; Morenzin, J.; Bechthold, P. S.; Gantefor, G.; Eberhardt, W.; Yang, D. S.; Hackett, P. A.; Fournier, R.; Pang, T.; Chen, C. F. *Phys. Rev. Lett.* **1996**, *77*, 4528−4531.
(15) Li, J.; Li, X.; Zhai, H.-J.; Wang, L.-S. *Science* **2003**, *299*, 864−867.
(16) Hakkinen, H.; Moseler, M.; Kostko, O.; Morgner, N.; Hoffmann, M. A.; Issendorff, B. v. *Phys. Rev. Lett.* **2004**, *93*, 093401.
(17) Kruckeberg, S.; Schooss, D.; Maier-Borst, M.; Parks, J. H. *Phys. Rev. Lett.* **2000**, *85*, 4494−4497.
(18) Maier-Borst, M.; Cameron, D. B.; Rokni, M.; Parks, J. H. *Phys. Rev. A* **1999**, *59*, R3162−R3165.
(19) Hall, B.; Flueli, M.; Monot, R.; Borel, J. P. *Helv. Phys. Acta* **1988**, *61*, 193−196.
(20) Hall, B. D.; Flueli, M.; Monot, R.; Borel, J. P. *Z. Phys. D: At., Mol. Clusters* **1989**, *12*, 97−101.
(21) Hall, B. D.; Flueli, M.; Monot, R.; Borel, J. P. *Phys. Rev. B* **1991**, *43*, 3906−3917.
(22) Reinhard, D.; Hall, B. D.; Ugarte, D.; Monot, R. *Z. Phys. D: At., Mol. Clusters* **1993**, *26*, S76−S78.
(23) Reinhard, D.; Hall, B. D.; Ugarte, D.; Monot, R. *Phys. Rev. B* **1997**, *55*, 7868−7881.
(24) Haberland, H.; Mall, M.; Moseler, M.; Qian, Y.; Reiners, T.; Thurner, Y. *J. Vac. Sci. Technol., A* **1994**, *12*, 2925−2930. An up to date version of the source can be found under deposition/experiment of http://www.fmf2.uni-freiburg.de/projekte/pg_cluster/projekt_cluster/haberland_e.html.
(25) Guan, S. H.; Marshall, A. G. *Int. J. Mass Spectrom. Ion Processes* **1996**, *158*, 5−37.
(26) Guan, S. H.; Marshall, A. G. *Anal. Chem.* **1993**, *65*, 1288−1294.
(27) *Stereochemical Applications of Gas-Phase Electron Diffraction*; Hargittai, I., Hargitta, M., Eds.; VCH: Weinheim, Germany, 1988.
(28) Bartell, L. S.; Kohl, D. A.; Carroll, B. L.; Gavin, R. M., Jr. *J. Chem. Phys.* **1965**, *42*, 3079−3084.
(29) Ahlrichs, R.; Baer, M.; Haeser, M.; Horn, H.; Koelmel, C. *Chem. Phys. Lett.* **1989**, *162*, 165−169.
(30) Eichkorn, K.; Weigend, F.; Treutler, O.; Ahlrichs, R. *Theor. Chem. Acc.* **1997**, *97*, 119−124.
(31) Eichkorn, K.; Treutler, O.; Oehm, H.; Haeser, M.; Ahlrichs, R. *Chem. Phys. Lett.* **1995**, *240*, 283−290.
(32) Becke, A. D. *Phys. Rev. A* **1988**, *38*, 3098−3100.
(33) Andrae, D.; Haussermann, U.; Dolg, M.; Stoll, H.; Preuss, H. *Theor. Chim. Acta* **1990**, *77*, 123−141.
(34) Doye, J. P. K.; Wales, D. J. *Phys. Rev. Lett.* **1998**, *80*, 1357−1360.
(35) Lloyd, L. D.; Johnston, R. L. *Chem. Phys.* **1998**, *236*, 107−121.
(36) Wales, D. J.; Doye, J. P. K.; Dullweber, A.; Hodges, M. P.; Naumkin, F. Y.; Calvo, F.; Hernández-Rojas, J.; Middleton, T. F. In *URL* http://www-wales.ch.cam.ac.uk/CCD.html.
(37) Bonacic-Koutecky, V.; Cespiva, L.; Fantucci, P.; Koutecky, J. *J. Chem. Phys.* **1993**, *98*, 7981−7994.
(38) Bonacic-Koutecky, V.; Cespiva, L.; Fantucci, P.; Pittner, J.; Koutecky, J. *J. Chem. Phys.* **1994**, *100*, 490−506.
(39) Fournier, R. *J. Chem. Phys.* **2001**, *115*, 2165−2177.
(40) Oviedo, J.; Palmer, R. E. *J. Chem. Phys.* **2002**, *117*, 9548−9551.

(41) Michaelian, K.; Rendon, N.; Garzon, I. L. *Phys. Rev. B* **1999**, *60*, 2000−2010.
(42) Doye, J. P. K.; Wales, D. J. *New J. Chem.* **1998**, *22*, 733−744.
(43) Jennison, D. R.; Schultz, P. A.; Sears, M. P. *J. Chem. Phys.* **1997**, *106*, 1856−1862.
(44) Marks, L. D. *Philos. Mag. A* **1984**, *49*, 81.
(45) The experimental Ag_2 distance is 2.5303 ± 0.00002 Å,[46] the DFT-distance is 2.575 Å.
(46) Beutel, V.; Kramer, H. G.; Bhale, G. L.; Kuhn, M.; Weyers, K.; Demtröder, W. *J. Chem. Phys.* **1993**, *98*, 2699−2708.
(47) Note added after submission: Recent TIED measurements by X. Xing et al. (*Phys. Rev. B* **2005**, *72*, 081405(R)) support our results for Ag_{55}^+.

NL0513434